



Cite this: *New J. Chem.*, 2018, 42, 20113

Two-acceptor one-donor random terpolymers comprising thiophene- and phenyl-capped diketopyrrolopyrrole for organic photovoltaics†

B. Sambathkumar,^{id}*^{ab} E. Varathan,^{id}^{abc} V. Subramanian^{id}^{ab} and N. Somanathan^{id}^{*ab}

A series of random terpolymers comprising two electron deficient phenyl (PDPP) and thiophene (ThDPP)-capped diketopyrrolopyrrole (DPP) in conjugation with the electron-donating thiophene moiety are synthesised using Stille coupling. Their optical properties, energy levels, hole mobility, crystallinity and solar cell device performance can be systematically fine-tuned by controlling the molar ratio between ThDPP/PDPP (30/70, 50/50, 70/30, and 90/10) contents in the polymer backbone. Herein, we find that the crystalline properties and hole mobility of the terpolymer are enhanced by increasing ThDPP content in the polymer backbone. However, increasing PDPP content leads to low hole mobility and weak crystalline features. These characteristic features afford remarkable effect on the solar cell device performance. Bulk heterojunction (BHJ) solar cells are constructed by using these random terpolymers as donor materials and [6,6]-phenyl-C₇₁-butyric acid methyl ester (PC₇₁BM) as the acceptor. The best device performances are obtained for polymer **P5T5P** with the ThDPP/PDPP ratio of 50/50 and power conversion efficiency (PCE) of 2.9% due to balanced charge carrier mobility and optimized crystallinity in addition to good miscibility and favorable surface morphology with the fullerene acceptor. This study demonstrates that improved control of the crystallinity of the polymer donor through structural engineering can greatly help in improving device performance.

Received 15th July 2018,
Accepted 29th October 2018

DOI: 10.1039/c8nj03536a

rs.c.li/njc

1. Introduction

There has been significant research interest in organic bulk heterojunction (BHJ) polymer solar cells (PSCs) as they are flexible and light in weight; the fabrication of large-area devices using various printing methodologies has led to BHJ as a promising next-generation renewable energy resource.^{1–4} In general, BHJs have a photoactive layer made up of a solid blend of conjugated polymers as the electron donor and fullerene derivatives such as [6,6]-phenyl-C₇₁-butyric acid methyl ester (PC₇₁BM) as the electron acceptor.^{5–7} This combination provides efficient charge separation and charge transport from the photo-generated exciton at the donor/acceptor interface.⁸ Recently, the power conversion efficiency (PCE) of PSCs has remarkably increased over 13% in single junctions and 17% in tandem structures.^{9–14} This is possibly due to the development of

low band gap-conjugated polymers consisting of electron-rich (donor, D) and electron-poor units (acceptor, A) arranged alternately in a polymer chain with a push-pull effect.^{15–17} One key challenge for improving PCE in PSCs is to develop new low-band-gap polymers with desired optoelectronic properties. Therefore conjugated polymers should exhibit broad and strong absorption for high short-circuit current density (J_{sc}), suitable HOMO and LUMO energy levels with fullerene derivatives for efficient exciton dissociation for high open-circuit voltage (V_{oc}) and favourable morphology and high charge transport for high FF. Hence, conjugated polymers have to balance these photovoltaic parameters for high PCE.^{18–23} However, only a limited number of D–A copolymers exhibit a high PCE value. In addition, all successful D–A alternate copolymers have a fixed D–A ratio (1:1), which further complicates the modification of the optoelectronic properties and device performance.^{24,25}

Recently, random Terpolymer design has been explored as a promising strategy for building ideal donor materials for BHJ solar cells.²⁶ The attractive advantage of terpolymer design is that the inclusion of additional comonomer units in the conjugated backbone provides complementary light absorption, which facilitates the harvesting of more photons, fine-tuning the energy level, band gap, charge transport ability, packing nature, and controlling solubility, crystallinity and miscibility with

^a CSIR-Central Leather Research Institute, Sardar Patel Road, Adyar, Chennai 600020, Tamil Nadu, India. E-mail: sambathkumarb@gmail.com

^b CSIR-Network of Institutes for Solar Energy, New Delhi, India

^c Department of Chemistry, Indian Institute of Technology Madras, Chennai 600036, Tamil Nadu, India

† Electronic supplementary information (ESI) available: This section contains detailed synthetic procedures for the monomers and copolymers, ¹H and ¹³C NMR, and MALDI mass spectra. See DOI: 10.1039/c8nj03536a

fullerene.^{27–31} Moreover, in random copolymerization, it is possible to fine-tune optical and electrical properties by varying donor or acceptor monomer composition stoichiometrically in the polymer backbone.^{32–37} However, the irregular arrangement of comonomer units in the polymer backbone raises the fundamental question about its molecular packing and charge transport nature.^{38,39} For instance, Janssen *et al.* synthesized random and regular terpolymers by copolymerizing DPP and thienopyrrolodione (TPD) in an alternate and random manner, and they reported that regular terpolymers exhibit high device performance compared to random polymers.⁴⁰ Therefore selecting a proper comonomer pair without disturbing its molecular packing and charge transport is crucial for designing a random terpolymer. For example, Jo *et al.* reported a series of 2A/1D-based random terpolymers by varying the comonomer compositions of Diketopyrrolopyrrole (DPP, A1) and Isoindigo (A2) randomly copolymerized with the thiophene unit in different ratios. They found that their carrier mobility and PCE was higher than that of the reference parent alternate regular polymer.⁴¹ In addition, the same group synthesized random terpolymers by tuning the composition of thiophene- and pyridine-flanked DPP copolymerized with bithiophene. The compositional terpolymer showed higher device performance with PCE of 8.11% and high hole mobility compared to the corresponding parent copolymer.⁴² Similarly, Kim *et al.* reported a series of terpolymers by randomly copolymerizing thiophene (Th) and selenophene (Se) with DPP; they systematically studied the effect of Th/Se ratio, and they found that increasing Se content enhanced the crystalline nature, which can lead to high mobility with the best PCE of 7.2% obtained for Se/Th (10/90).⁴³

Among various acceptor units, DPP units are widely investigated due to their high extension coefficient, electron-deficient lactam group, rigid planar molecular skeleton favouring strong intermolecular π - π interaction, absorption in the near-infrared (NIR) region and high charge transport nature. Moreover, thiophene-flanked DPP (ThDPP) polymers exhibit low band gaps with absorption in the near-infrared (NIR) region and show high J_{sc} and favourable morphology for charge transport.^{44–46} Phenyl-flanked DPP (PDPP) units show medium band gaps with strong absorption in the visible region and exhibit deep HOMO levels, which favour higher V_{oc} .^{47–50}

Based on the above consideration, here, we synthesized and characterized a series of random terpolymers comprising both ThDPP and PDPP units copolymerized randomly with thiophene units using Stille polymerization. By systematically varying the composition of ThDPP and PDPP units in a polymer backbone, it is possible to fine-tune the optical and electrical properties of terpolymers. A systematic analysis is reported for their structure-property relationship using optical, electrochemical, thermal, electrical, density functional theory calculations and photovoltaic study.

2. Experimental section

2.1 Materials

2-Thiophenecarbonitrile, 4-bromobenzonitrile, dimethyl succinate, potassium *tert*-butoxide, 2-methyl-2-butanol, tri(*o*-tolyl)phosphine,

N-bromosuccinimide (NBS), 2,5-bis(trimethylstannyl)thiophene, tris(dibenzylideneacetone)dipalladium(0), Aliquat, anhydrous toluene, chloroform-*d* and 1,1,2,2-tetrachloroethane-*d*₂ were purchased from Aldrich Chemical Company and used without any further purification.

2.2 Instrumentation methods

¹H and ¹³C NMR spectra were recorded on a Bruker 400 MHz NMR spectrometer. UV-Visible absorption spectra were recorded on a Varian Carey 50 Bio UV-Visible spectrophotometer. Elemental analyses for the polymers were performed on a Euro Vector S.P.A, Euro EA 3000 CHNS Elemental Analyzer. Cyclic voltammetry (CV) measurements were performed using a CHI 600D electrochemical workstation. CV measurements were carried out in 0.1 M tetrabutylammonium hexafluorophosphate (TBAPF6) acetonitrile solution using a platinum disc electrode as the working electrode, an Ag/AgCl electrode as the reference electrode and a platinum wire electrode as the counter electrode. For CV measurements, the polymer was dissolved in chloroform solution and coated on a platinum disc with a concentration of 1 mg mL⁻¹. Thermal analysis was carried out using Mettler TOLEDO TGA/SDTA 851e at a heating rate of 10 °C min⁻¹. X-ray diffraction (XRD) measurements were carried out using a Bruker AXS D8 Advance X-ray diffractometer at a wavelength of (1.5464 Å). The surface morphologies were observed by atomic force microscopy (AFM) on a Nova 1.0.26 RC1 in semi contact mode with NT-MDT solver software.

2.3 Solar cell and mobility measurement

The ITO-coated glass substrates were cleaned by ultrasonication sequentially in detergent, deionized water, acetone and isopropyl alcohol for 15 minutes and dried in an oven at 80 °C for 12 hours. A thin layer of poly(3,4-ethylenedioxythiophene):poly(styrene sulfonate) (PEDOT:PSS; Clevis P VP Al 4083) as a hole transport layer was spin-coated at 3000 rpm and dried at 110 °C for 20 minutes. The blending solution was prepared by taking the polymer and PCBM in the ratio of 1:2 (18 mg mL⁻¹) in chloroform/*ortho*-dichlorobenzene (CF/*o*-DCB; 90:10) as the co-solvent mixture. The blending solution was spin-coated onto the ITO/PEDOT:PSS layer at 800 rpm for 60 s under N₂ environment. The active layer thickness was approximately ~100 nm. Finally, 1 nm of LiF and 100 nm of Al were thermally deposited at a pressure of approximately 1 × 10⁻⁶ Torr. The effective device area of the cell was 0.08 cm². The current density-voltage characterization was studied using a Keithley 2400 source measure unit. The photocurrent was measured using a Xe lamp source under 1 sun AM 1.5 solar illumination.

The hole-only device was fabricated using a device configuration of ITO/PEDOT:PSS (30 nm)/polymer (50 nm)/Au (100 nm). Hole mobility was calculated from the dark current density-voltage (*J*-*V*) curve by fitting the space-charge-limited current (SCLC) model using the Mott-Gurney equation

$$J = \frac{9}{8} \mu \epsilon_0 \epsilon_r \frac{(V)^2}{d^3}$$

where *J* is the current density, *d* is the film thickness of the active layer, μ is the hole mobility, ϵ_r is the relative dielectric constant

(assumed as 2.75 for conjugated polymers) of the transport medium, ϵ_0 is the permittivity of free space ($8.854 \times 10^{-12} \text{ F m}^{-1}$), d is the thickness of the polymer and V is the effective voltage.

3. Results and discussion

3.1 Synthesis

The chemical structures of the four terpolymers are shown in Fig. 1, and their synthetic routes are outlined in Scheme 1. The terpolymers were synthesized by copolymerizing ThDPP, PDPP and 2,5-bis(trimethylstannyl)thiophene using palladium-catalyzed Stille polymerization at 100°C for 24 hours in toluene. The different molar feed ratios of comonomers 50:50, 70:30, 30:70 and 90:10 (ThDPP/PDPP) and their respective terpolymers are named as **P5T5P**, **P7T3P**, **P3T7P** and **P9T1P**. The feed ratio of the terpolymer was determined by NMR spectra. The detailed

synthetic procedures of the corresponding monomer and terpolymer are discussed in the ESI.† All the terpolymers exhibited good solubility in common organic solvents such as tetrahydrofuran, dichloromethane, chloroform, toluene, chlorobenzene and 1,2-dichlorobenzene. Gel permeation chromatography (GPC) was performed to determine the weight-average molecular weight (M_w), number-average molecular weight (M_n), and polydispersity index (PDI) in tetrahydrofuran solution relative to that of the polystyrene standard, and the results are tabulated in Table 1.

3.2 Optical properties

The photophysical properties of random terpolymers were investigated using UV-Visible (UV-Vis) spectroscopy. Fig. 2 displays the absorption spectra of terpolymers in dilute chloroform solution and thin films, and their corresponding optical parameters are

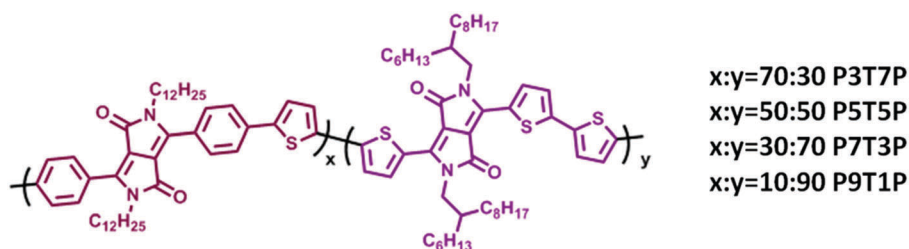
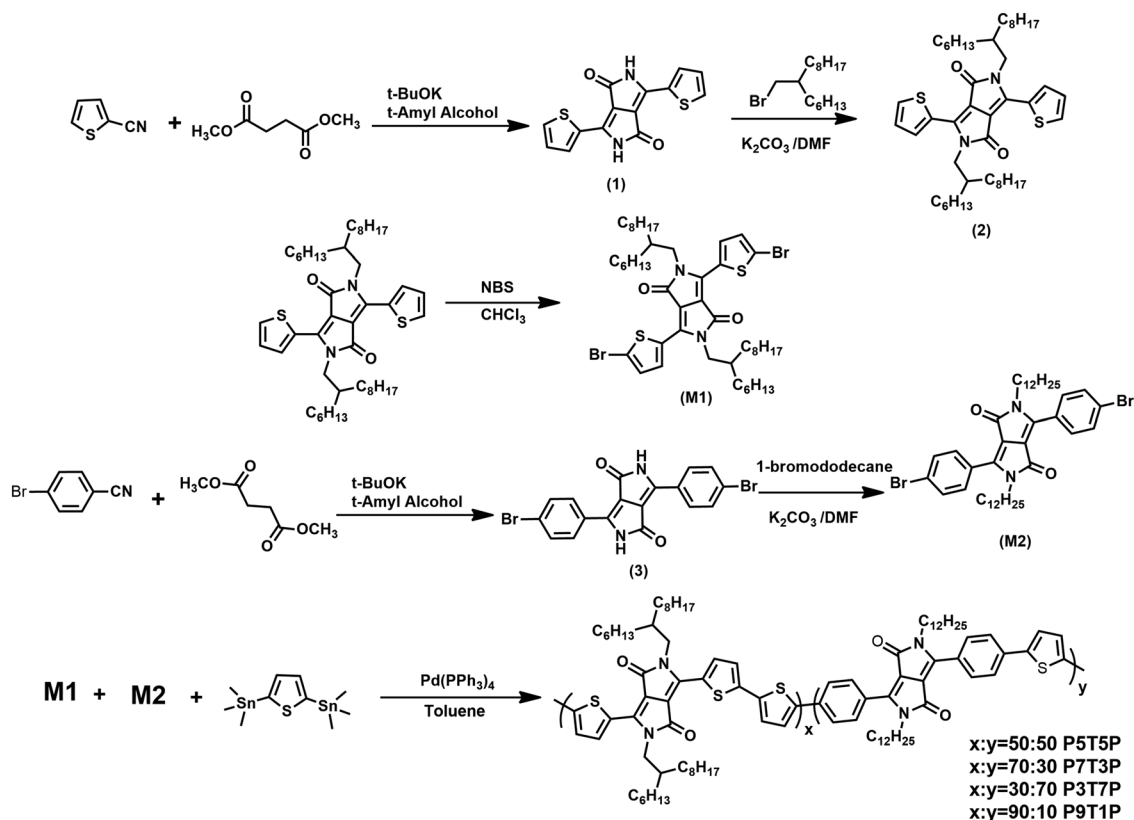


Fig. 1 Chemical structures of random terpolymers **P3T7P**, **P5T5P**, **P7T3P** and **P9T1P**.



Scheme 1 Synthesis route of monomer and terpolymer.

Table 1 Optical and thermal properties and molecular weight characterization of terpolymers

Polymer	λ_{\max}^a (nm) (solution)	λ_{\max}^b (nm) (thin film)	$E_{g(\text{opt})}^c$ (eV) (thin film)	T_d^d ($^{\circ}\text{C}$)	M_n^e (kg mol^{-1})	M_w^f (kg mol^{-1})	Dispersity (D)
P3T7P	346, 399, 563, 639	367, 403, 580, 641, 697	1.47	463	32.7	103.0	3.14
P5T5P	401, 696	407, 716	1.38	454	92.4	204.1	2.21
P7T3P	399, 722	403, 753	1.31	429	49.4	182.0	3.68
P9T1P	419, 793	410, 823	1.30	431	38.0	111.0	2.92

^a Absorption in CHCl_3 solution. ^b Absorption for thin films on quartz. ^c Optical band gap calculated from the onset of the thin film. ^d 5% weight loss temperature measured by TGA under N_2 . ^e Number-average molecular weight. ^f Weight-average molecular weight.

summarized in Table 1. In both the solution and the thin film, all the terpolymers exhibited two distinct absorption bands. The absorption band in the lower wavelength region (350 to 450 nm) corresponded to localized π - π^* transition (LT), and the band in the higher wavelength region (500–1000 nm) was ascribed to intramolecular charge transfer (ICT) from the donor to the acceptor. In thin films, λ_{\max} for polymer **P9T1P** was observed at 823 nm, which was ~ 240 nm longer than that of **P3T7P** (580 nm), ~ 70 nm longer than that of **P7T3P** (753 nm) and ~ 100 nm longer than that of **P5T5P** (716 nm). This finding illustrates that increasing the ThDPP comonomer unit in the polymer backbone results in a red shift in the long wavelength region. This is probably due to heteroatom interaction ($\text{S}\cdots\text{O}$) between the lactam oxygen and the adjacent sulphur unit in thiophene, facilitating a high degree of coplanar conformation and electron donating nature of the thiophene unit in ThDPP when compared to that for PDPP.⁵¹ This feature helps enhance strong intermolecular π - π interactions and highly-ordered packing, which is the reason for this dramatic red shift in absorption.⁵² Furthermore, compared to the solution, in the thin film, all the terpolymers show broad absorption as well as red shifts in both absorption maxima and onset, which are due to the strong aggregating nature in the thin film. From the onset of thin film absorption, the optical band gaps $E_{g(\text{opt})}^{\text{opt}}$ are 1.47, 1.38, 1.31 and 1.30 eV for **P3T7P**, **P5T5P**, **P7T3P** and **P9T1P**, respectively. Thus, it is possible to fine-tune the absorption maxima and band gap by regulating the molar ratio of PDPP and ThDPP units in a polymer chain.

3.3 Thermal properties

The thermogravimetric (TGA) thermograms of this terpolymer are shown in Fig. 3, and the corresponding decomposition

temperatures (T_d) of terpolymer are summarized in Table 1. The T_d values of polymers **P3T7P**, **P5T5P**, **P7T3P** and **P9T1P** are 463, 454, 429 and 431 $^{\circ}\text{C}$, respectively. As determined from the T_d value, increasing PDPP monomer content on the polymer backbone enhances the thermal stability of the terpolymer.⁵³ In addition, all the terpolymers exhibit good thermal stability, which is essential for device fabrication and photovoltaic application.

3.4 Electrochemical properties

To study the HOMO, LUMO and electrochemical band gap of the copolymer, cyclic voltammetry (CV) analysis was performed on a copolymer coated onto a Pt electrode as the working electrode in 0.1 M tetrabutylammonium hexafluorophosphate (Bu_4NPF_6) solution of acetonitrile as a supporting electrolyte. For calibration, the ferrocene/ferrocenium ion (Fc/Fc^+) redox couple was used as an external standard with a potential of 0.40 V against the (Ag/Ag^+) potential, assuming the redox potential of Fc/Fc^+ to have an absolute energy level of -4.80 eV in vacuum. Based on their first onset oxidation potential (E_{ox}) and the reduction potential (E_{red}), the corresponding HOMO and LUMO energy levels of the copolymer were calculated.⁵⁴ The CV curves are shown in Fig. 4, and their corresponding HOMO, LUMO and electrochemical band gap are summarized in Table 2. The HOMO energy levels of copolymers **P3T5P**, **P5T5P**, **P7T3P** and **P9T1P** were -5.44 , -5.36 , 5.31 , and -5.25 eV, respectively. These values clearly imply that increasing the phenyl-flanked DPP unit in the polymer backbone lowers the HOMO value due to the weak electron-donating ability of phenyl compared to that of the thiophene unit.⁵⁵

However, there is not much variation in the LUMO energy levels of all the copolymers, suggesting that LUMO is mainly

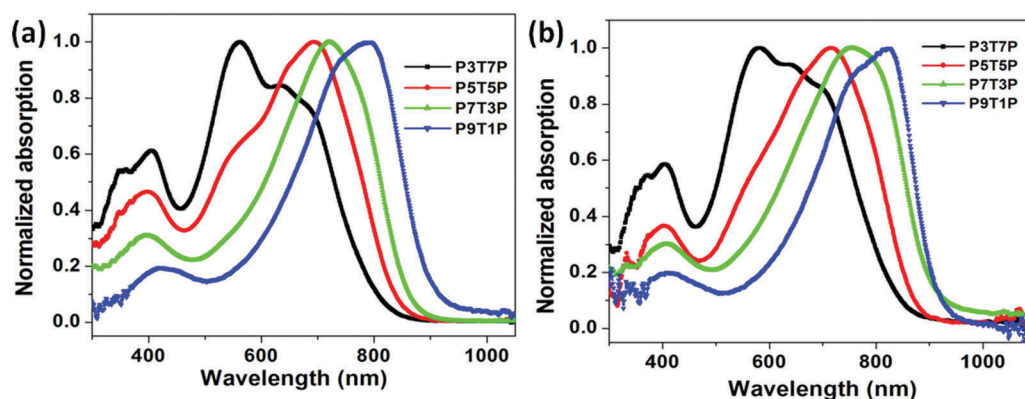


Fig. 2 Absorption spectra of terpolymers in (a) dilute chloroform solution (b) thin film.

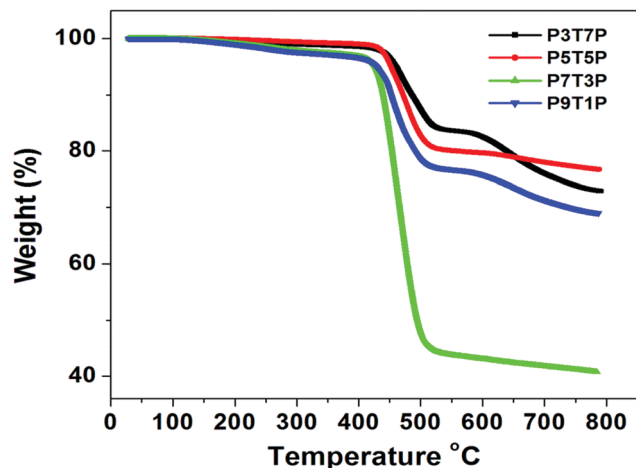


Fig. 3 TGA thermograms of terpolymers recorded at a heating rate of $10\text{ }^{\circ}\text{C min}^{-1}$ under N_2 atmosphere.

controlled by the DPP unit. The LUMO energy levels of copolymers **P3T5P**, **P5T5P**, **P7T3P** and **P9T1P** are -3.85 , -3.89 , -3.92 and -3.92 eV, respectively, which are significantly larger than the LUMO of PCBM (*ca.* 4.2 eV). These LUMO offsets (~ 0.3 eV) provide a sufficient driving force for efficient exciton dissociation and charge transfer with fullerene derivatives.⁵⁶ The electrochemical band gaps (E_g^{ec}) of the copolymers are calculated based on whether their LUMO and HOMO difference is in the range from 1.59 to 1.33 eV, which is slightly larger than the optical band gap E_g^{opt} probably due to the high exciton binding energy of the organic conjugated material.⁵⁷ The above results reveal that by varying the copolymer composition in the

Table 2 Electrochemical characterization of polymers

Polymer	$E_{\text{ox}}/E_{\text{red}}$	HOMO ^a (eV)	LUMO ^a (eV)	E_g^{ec} ^b (eV)
P3T7P	$-1.04/-0.55$	-5.44	-3.85	1.59
P5T5P	$-0.96/-0.51$	-5.36	-3.89	1.47
P7T3P	$-0.91/-0.48$	-5.31	-3.92	1.39
P9T1P	$-0.85/-0.48$	-5.25	-3.92	1.33

^a Calculated according to the formula $\text{HOMO/LUMO} = -e(E_{\text{ox/red}} + 4.40)$ (eV). ^b $E_g^{\text{ec}} = (\text{LUMO} - \text{HOMO})$.

polymer backbone, it is possible to adjust the HOMO/LUMO energy levels and band gaps of copolymers.

3.5 Theoretical calculation

To understand the composition effect of ThDPP/PDPP on the molecular geometry and electronic properties of copolymers, three model systems were studied with different arrangements in monomer sequence. The ground state geometries were optimized using density functional theory (DFT) at the B3LYP/6-31G* level of theory, as implemented in the Gaussian 09 package.⁵⁸ All the optimized structures were characterized by frequency analysis and were shown to be positive frequencies. To simplify the simulation, the long alkyl group on the DPP unit was replaced by a methyl group.⁵⁹ The optimized geometries, chemical structures, dihedral angles and electron density contour plots of HOMO and LUMO are displayed in Fig. 5. It can be noted from Fig. 5 that for the PDPP-Th-ThDPP model system, the dihedral angle between PDPP and Th unit is 19° , whereas a value of 10° was observed for Th and ThDPP. Therefore, the interfacial angle between the ThDPP and PDPP units is $\sim 30^{\circ}$. Upon adding one more ThDPP unit into

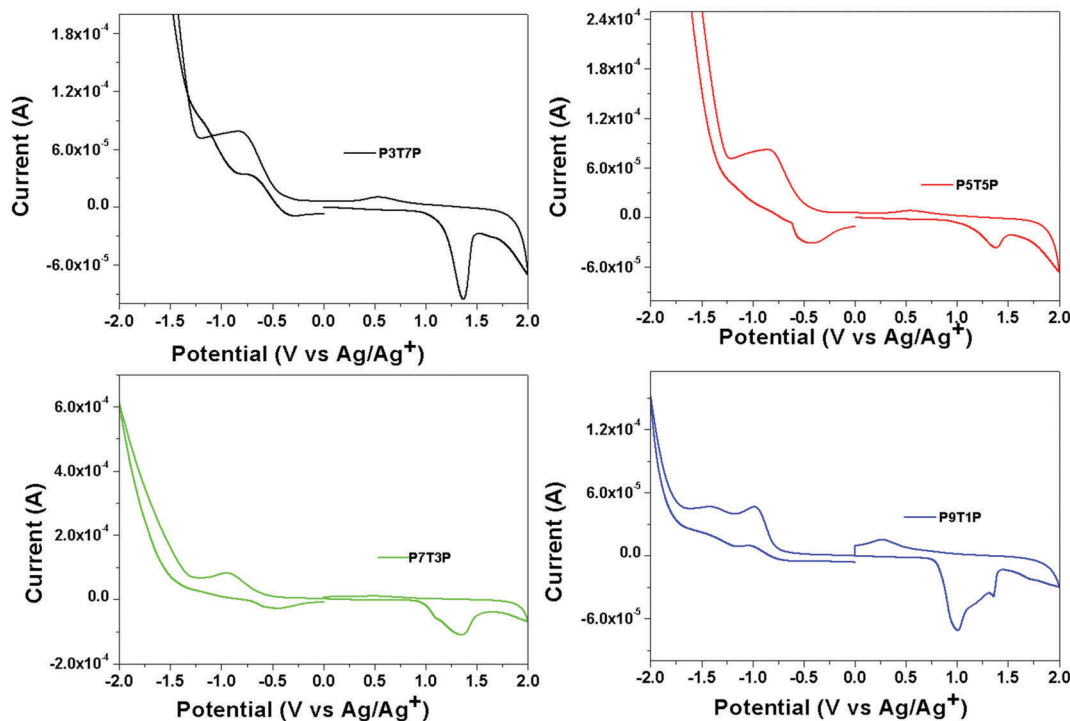


Fig. 4 Cyclic voltammograms of terpolymers in thin films.

the PDPP-Th-ThDPP core, the dihedral angle between the ThDPP and PDPP units in the resultant modelled system (PDPP-Th-ThDPP-Th-ThDPP) was marginally altered (from $\sim 30^\circ$ to $\sim 25^\circ$). Similarly, by adding one more PDPP unit into the PDPP-Th-ThDPP core, the dihedral angle between two adjacent PDPP units in the resultant modelled system (PDPP-Th-PDPP-Th-ThDPP) exhibited a high value of $\sim 40^\circ$, which was two times larger than that for two adjacent ThDPP ($\sim 20^\circ$). The preceding discussion clearly reveals that increasing the ThDPP unit in the polymer backbone increases molecular planarity in the co-polymer, which facilitates intermolecular interaction and conjugation strength. These results are in good agreement with the results of absorption and XRD analyses. Electron density contour plots (Fig. 5) indicate that for PDPP-Th-ThDPP, the electron density of HOMO is mainly delocalized on Th and ThDPP units with negligible contribution from PDPP. On the other hand, the electron density distribution of LUMO is completely delocalized on whole units, favouring LUMO stabilization. These features confirm an intramolecular charge-transfer transition between ThDPP and PDPP units. Similar HOMO and LUMO electron density distributions are observed in PDPP-Th-PDPP-Th-ThDPP, which indicates that the addition of PDPP does not affect the electron density distribution. In case of the PDPP-Th-ThDPP-Th-ThDPP model system, both HOMO and LUMO electron densities are delocalized on ThDPP units.

3.6 XRD analysis

To evaluate the effect of the PDPP:ThDPP ratio in a polymer, we performed lamellar ordering and π - π stacking arrangement X-ray diffraction (XRD) analysis for the copolymers in thin films. Their XRD patterns are shown in Fig. 6. At small angle values, all the copolymers show first-order, second-order and third-order diffraction peaks at a ratio of 1:2:3, indicating long-range-ordered lamellar arrangement.^{60–62} The first-order lamellar stacking peak for the terpolymer exists at around $2\theta = 4.6$ – 4.46 , which corresponds to the lamellar spacing distance from 19 to 19.78 Å. Even though there are no significant variations

in their lamellar spacing arrangements, the first-order peak for **P9T1P** shows high intensity compared to that of the other three polymers. Similarly, second- and third-order diffraction patterns also follow a similar trend. In addition, in the wide-angle region, additional diffraction peaks are observed at $2\theta = 24.00^\circ$, 23.79° , 23.51° and 23.24° for **P5T5P**, **P7T3P**, **P3T7P** and **P9T1P**, which correspond to *d* spacings of 3.70 Å, 3.73 Å, 3.78 Å and 3.83 Å, indicating π - π stacking between the polymer backbone. The π - π stacking distances of the copolymers can be ranked in the order of **P9T1P** < **P7T3P** < **P5T5P** < **P3T7P**, indicating that copolymer **P9T1P** has a shorter π - π distance compared to others. From the XRD peak intensities, we infer that **P9T1P** displays an intense diffraction pattern in both the small-angle and wide-angle regions, and the diffraction intensities of the copolymers are ranked in the order of **P9T1P** > **P7T3P** > **P5T5P** > **P3T7P**. Thus, the XRD result clearly explains that increasing ThDPP content in the polymer backbone enhances crystalline behaviour and π - π stacking. To further understand the nanostructure of the blend films, XRD analysis is carried out. It is clear from Fig. 6 that intermixing PC₇₁BM moieties with the polymer disrupts blend crystallization due to the effect of PC₇₁BM intercalation. However, their lamellar spacing arrangements and π - π stacking distances are nearly the same as those of pristine terpolymers.

3.7 Hole mobility

To further explore the composition effect of ThDPP/PDPP content in the terpolymers on their electrical performance, hole mobility measurements were obtained for pristine copolymers using the space charge limit current (SCLC) method. The hole mobility values of pristine copolymers are calculated from the current density–voltage (*J*-*V*) curves. Fig. 7 depicts their log-log current (*J*-*V*) plots, and their mobility data are summarized in Table 3. The hole motilities of **P3T7P**, **P5T5P**, **P7T3P**, **P9T1P** are 1.9×10^{-6} , 7.8×10^{-6} , 2.1×10^{-5} and 3.4×10^{-5} cm² V⁻¹ s⁻¹, respectively. From the values, it is clear that increasing ThDPP content in the polymer backbone helps increase the mobility.

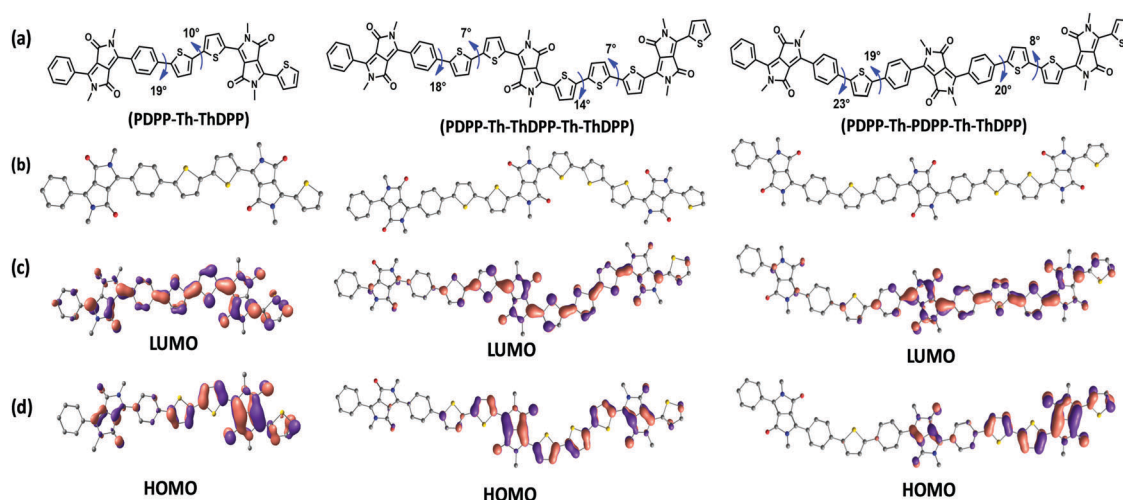


Fig. 5 Chemical structures and their corresponding dihedral angles (a), optimized geometries (b), pictorial representations of the optimized molecular orbitals of LUMO (c) and HOMO (d) of the modeled oligomers obtained at the B3LYP/6-31G* level of theory.

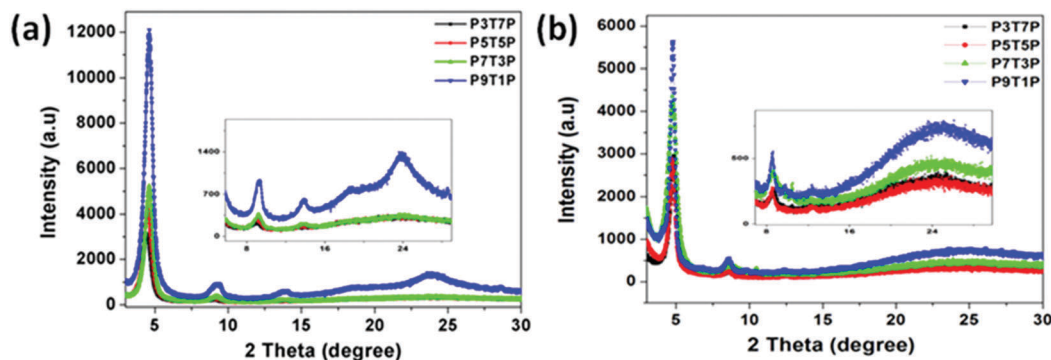


Fig. 6 XRD patterns of (a) pristine terpolymers and (b) blend films.

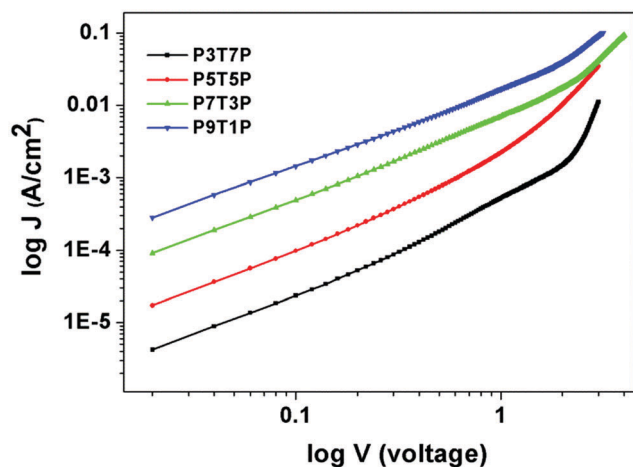


Fig. 7 Hole mobility of pristine terpolymers in thin films.

Notably, **P9T1P** shows a higher mobility value compared to their analogue copolymer probably due to its stronger crystalline behaviour and more rigid characteristics, which is in good agreement with the results of XRD and DFT characterizations.

3.8 Photovoltaic properties and morphological behaviour

The photovoltaic performances of the terpolymers were investigated by fabricating BHJ PSCs with the conventional device structure of ITO/PEDOT:PSS (40 nm)/polymer:PC₇₁BM (100 nm)/LiF (1 nm)/Al (100 nm). The optimal weight ratio of polymer:PC₇₁BM was 1:2 (wt%) with a total concentration of 18 mg mL⁻¹ in a mixed co-solvent of CF:ODCB (9:1). Fig. 8 illustrates the *J-V* characteristics and external quantum efficiency (EQE) of the

terpolymers, and their photovoltaic parameters are tabulated in Table 3. The V_{oc} values of the random copolymers are ranked in the order of **P9T1P** (0.51V) < **P7T3P** (0.59 V) < **P5T5P** (0.60 V) < **P3T7P** (0.70 V). The variations observed in the V_{oc} values of the terpolymers are in good agreement with the HOMO energy level of the terpolymers since V_{oc} is directly proportional to the HOMO energy level of the polymer donor and the LUMO energy level of the PC₇₁BM acceptor unit.^{63,64} Therefore, polymers with lower HOMO energy levels show higher V_{oc} . Moreover a nonlinear composition dependence was observed in the PCE of the terpolymers from 0.54% to 2.9% in the order of **P5T5P** (2.9%) > **P7T3P** (1.38%) > **P9T1P** (1.18%) > **P3T7P** (0.54%). Specifically, **P5T5P** showed the highest PCE value of 2.9% (V_{oc} = 0.59 V; J_{sc} = 12.3 mA cm⁻²; and FF = 39) among all the terpolymers. However, polymers with higher ThDPP (**P7T3P** and **P9T1P**) content, which show higher hole mobility, provided poor device performance. Similarly, **P3T7P** with higher PDPP content showed poor PCE probably due to its lower hole mobility and poor crystallinity, which is in accordance with SCLC measurement and XRD analysis.

To determine the variation in the current density of the polymer/PC₇₁BM-based device, external quantum efficiencies (EQEs) were measured under optimized conditions and are shown in Fig. 8b. The measured EQE spectra are in good agreement with the optical absorption and *J-V* curves. Notably, the **P5T5P**/PC₇₁BM device showed a good spectral coverage from 300 to 900 nm with maximum EQE values of ~63% at 370 nm, ~41% at 550 nm and 33% at 760 nm due to its high J_{sc} value. **P7T3P** and **P9T1P** showed low EQE values compared to **P5T5P**, whereas **P3T7P** showed extremely low EQE values with poor spectral coverage, indicating their poor device performance. Thus, higher EQE with broad spectral coverage

Table 3 Photovoltaic properties of polymer/PC₇₁BM under optimized conditions and hole mobility measurements of the pristine polymer under dark conditions

Polymer	V_{oc} (V)	J_{sc} (mA cm ⁻²)	FF	PCE	μ_{th} (cm ⁻² V ⁻¹ s ⁻¹)
P3T7P	0.71 ± 0.03	4.1 ± 0.2	19 ± 3	0.55 ± 0.1	1.9(±0.5) × 10 ⁻⁶
P5T5P	0.60 ± 0.02	12.3 ± 0.3	39 ± 2	2.9 ± 0.3	7.8(±0.4) × 10 ⁻⁶
P7T3P	0.59 ± 0.01	5.2 ± 0.1	45 ± 1	1.38 ± 0.08	2.1(±0.1) × 10 ⁻⁵
P9T1P	0.51 ± 0.02	6.3 ± 0.1	36 ± 2	1.16 ± 0.15	3.4(±0.3) × 10 ⁻⁵

The weight ratio of polymer/PC₇₁BM was 1:2, and the average values (4 devices; 16 individual pixels) are shown with standard deviation.

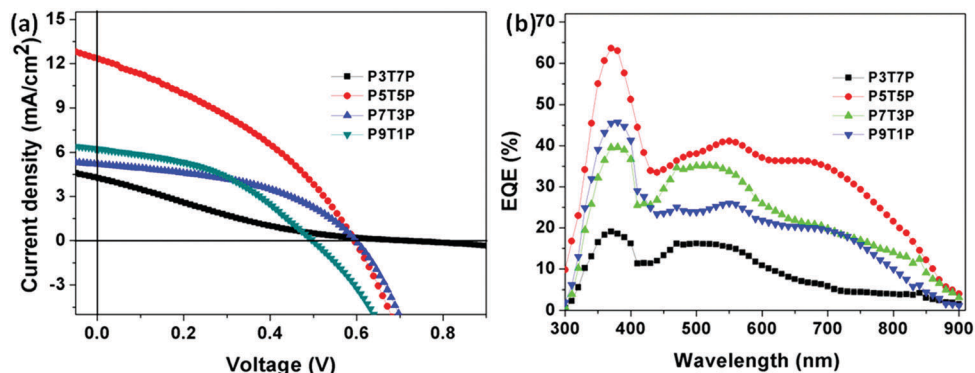


Fig. 8 Current–voltage (J – V) curves (a) and EQE spectra (b) of the polymer:PC₇₁BM blend under optimized conditions.

promoted **P5T5P**/PC₇₁BM-based devices for higher J_{sc} values compared to others.

To deeply examine discrepancies in the photovoltaic performances of the polymers/PC₇₁BM blend films, atomic force microscopy (AFM) analyses are performed based on their device configuration. The AFM images of the blend films are shown in Fig. 9. The root-mean-square (RMS) surface roughness values of the **P5T5P**, **P7T3P**, **P3T7P** and **P9T1P** blend films are 0.96 nm, 1.89 nm, 6.51 nm and 7.16 nm, respectively. **P5T5P** and **P7T3P** show lower RMS values with smooth surface

roughness compared to **P3T7P** and **P9T1P**; in particular, **P5T5P** shows finer phase separation compared to **P7T3P**.^{65,66} This distinctive morphology favours higher device performance and J_{sc} values, whereas **P3T7P** shows ill-defined morphology with about ~ 300 nm-sized spherical structures that are unfavorable for exciton migration and separation toward the polymer/fullerene interface, eventually decreasing PCE and J_{sc} (4.1 mA cm^{-2}).⁶⁷ In contrast, **P9T1P** shows fibril bundle with macro-phase separation and is more homogeneously distributed with a high RMS value probably due to its highly

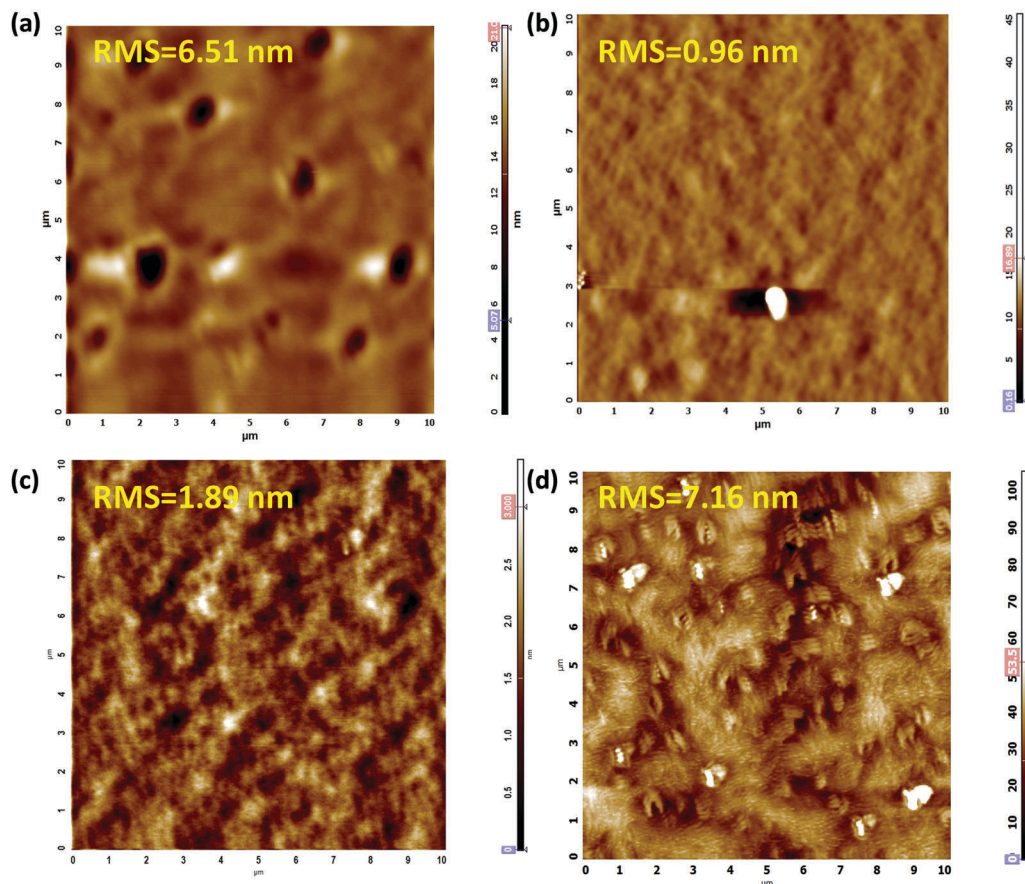


Fig. 9 AFM height images of (a) **P3T7P**, (b) **P5T5P**, (c) **P7T3P**, and (d) **P9T1P** blend films under optimized conditions.

crystalline nature, which favours polymer chain aggregation, resulting in poor miscibility and lower device performance.⁶⁸

4. Conclusions

In conclusion, a series of random terpolymers comprising two electron deficient phenyl- and thiophene-capped DPP units of various compositions were synthesised. By using random terpolymer strategy, we fine-tune the physical properties of the terpolymers such as the absorption spectrum, HOMO/LUMO energy levels, band gap, mobility, crystallinity and morphology, which are directly related to photovoltaic device performance. Increasing ThDPP content in the polymer backbone drastically enhances crystallinity and mobility, which are major factors for device performance, whereas increasing PDPP causes poor hole mobility due to its non-planar conformation between the phenyl and DPP moieties. The DFT studies also reveal that a large dihedral angle is observed between the phenyl and DPP units; in addition, the XRD patterns also provide weak crystalline characteristics for higher PDPP content-based terpolymers. The enhanced crystallinities and hole mobilities of the terpolymers are ranked in the order of **P9T1P** > **P7T3P** > **P5T5P** > **P3T7P**. However, a non-linear trend is observed in solar cell device performance since the crystallinity of the terpolymer strongly influences the morphology; the polymers self-aggregate, leading to poor miscibility with fullerene, which results in macro-phase separation as the ThDPP content is increased. Therefore, polymer **P5T5P** (PDPP:ThDPP = 50:50) with optimal device morphology and balanced hole mobility shows better device performance with PCE of 2.9% with an open-circuit voltage (V_{oc}) of 0.60 V, a short-circuit current (J_{sc}) of 12.3 mA cm⁻², and a fill factor (FF) of 39%. Thus, the random terpolymer approach affords a potential strategy to optimize the physical properties and device performances of terpolymers.

Conflicts of interest

There are no conflicts to declare.

Acknowledgements

The authors thank CSIR-NWP 54 for their financial support through the TAPSUN project. E. V. thanks SERB for NPDPF (PDF/2017/000059). The authors would also like to thank Dr A. Ajayaghosh, J. D. Sudha, and R. Ramakrishnan (NIIST, Trivandrum, India) for the AFM measurements. The authors sincerely thank Prof. Dr R. Damodaran and Mr E. Ramachandran (Department of Chemistry, IIT Madras) for their timely help.

References

- L. Dou, J. You, Z. Hong, Z. Xu, G. Li, R. A. Street and Y. Yang, *Adv. Mater.*, 2013, **25**, 6642–6671.
- M. C. Scharber and N. S. Sariciftci, *Prog. Polym. Sci.*, 2013, **38**, 1929–1940.
- H. F. Dam, T. R. Andersen, M. V. Madsen, T. K. Mortensen, M. F. Pedersen, U. Nielsen and F. C. Krebs, *Sol. Energy Mater. Sol. Cells*, 2015, **140**, 187–192.
- S. Berny, N. Blouin, A. Distler, H. J. Egelhaaf, M. Krompiec, A. Lohr, O. R. Lozman, G. E. Morse, L. Nanson, A. Pron, T. Sauermaun, N. Seidler, S. Tierney, P. Tiwana, M. Wagner and H. Wilson, *Adv. Sci.*, 2016, **3**, 1500342.
- A. J. Heeger, *Adv. Mater.*, 2014, **26**, 10–28.
- J. Nelson, *Mater. Today*, 2011, **14**, 462–470.
- G. Li, R. Zhu and Y. Yang, *Nat. Photonics*, 2012, **6**, 153–161.
- C. M. Proctor, M. Kuik and T.-Q. Nguyen, *Prog. Polym. Sci.*, 2013, **38**, 1941–1960.
- W. Zhao, S. Li, S. Zhang, X. Liu and J. Hou, *Adv. Mater.*, 2017, **29**, 1604059.
- Z. Xiao, X. Jia and L. Ding, *Sci. Bull.*, 2017, **62**, 1562–1564.
- H. Li, Z. Xiao, L. Ding and J. Wang, *Sci. Bull.*, 2018, **63**, 340–342.
- J. Zhang, L. Zhu and Z. Wei, *Small Methods*, 2017, **1**, 1700258.
- X. Che, Y. Li, Y. Qu and S. R. Forrest, *Nat. Energy*, 2018, **3**, 422–427.
- L. Meng, Y. Zhang, X. Wan, C. Li, X. Zhang, Y. Wang, X. Ke, Z. Xiao, L. Ding, R. Xia, H.-L. Yip, Y. Cao and Y. Chen, *Science*, 2018, **361**, 1094–1098.
- H. Zhou, L. Yang and W. You, *Macromolecules*, 2012, **45**, 607–632.
- L. Bian, E. Zhu, J. Tang, W. Tang and F. Zhang, *Prog. Polym. Sci.*, 2012, **37**, 1292–1331.
- T. Xu and L. Yu, *Mater. Today*, 2014, **17**, 11–15.
- Y. Li, *Acc. Chem. Res.*, 2012, **45**, 723–733.
- B. Qi and J. Wang, *J. Mater. Chem.*, 2012, **22**, 24315–24325.
- X. Guo, M. Baumgarten and K. Müllen, *Prog. Polym. Sci.*, 2013, **38**, 1832–1908.
- L. Dou, Y. Liu, Z. Hong, G. Li and Y. Yang, *Chem. Rev.*, 2015, **115**, 12633–12665.
- C. L. Chochos and S. A. Choulis, *Prog. Polym. Sci.*, 2011, **36**, 1326–1414.
- B. Hemavathi, T. N. Ahipa and R. K. Pai, *Eur. Polym. J.*, 2015, **72**, 309–340.
- R. Po and J. Roncali, *J. Mater. Chem. C*, 2016, **4**, 3677–3685.
- T. E. Kang, K. H. Kim and B. J. Kim, *J. Mater. Chem. A*, 2014, **2**, 15252–15267.
- L. Ye, X. Jiao, S. Zhang, H. Yao, Y. Qin, H. Ade and J. Hou, *Adv. Energy Mater.*, 2016, 1601138.
- M. L. Keshtov, A. R. Khokhlov, S. A. Kuklin, S. A. Osipov, N. A. Radychev, M. I. Buzin and G. D. Sharma, *Org. Electron.*, 2017, **41**, 1–8.
- R. Hou, B. Zhao, F. Wu, G. Wang, T. Shen, H. Guo, J. Zhang, H. Chen and S. Tan, *Org. Electron.*, 2015, **20**, 142–149.
- S. Ko, R. Mondal, C. Risko, J. K. Lee, S. Hong, M. D. McGehee, J. L. Bredas and Z. Bao, *Macromolecules*, 2010, **43**, 6685–6698.
- B. Sambathkumar, P. S. V. Kumar, F. S. Deepakrao, S. S. K. Iyer, V. Subramanian, R. Datt, V. Gupta, S. Chand and N. Somanathan, *J. Phys. Chem. C*, 2016, **120**, 26609–26619.
- S. Goker, G. Hizalan, E. Aktas, S. Kutkan, A. Cirpanabde and L. Toppare, *New J. Chem.*, 2016, **40**, 10455–10464.

- 32 T. E. Kang, H. H. Cho, H. J. Kim, W. Lee, H. Kang and B. J. Kim, *Macromolecules*, 2013, **46**, 6806–6813.
- 33 V. Tamilavan, Y. Liu, R. Agneeswari, D. Y. Lee, S. Cho, Y. Jin, S. H. Park and M. H. Hyun, *Polymer*, 2016, **95**, 18–25.
- 34 T. Jiang, Y. Yang, Y. Tao, C. Fan, L. Xue, Z. Zhangrandom, H. Li, Y. Li and W. Huang, *Polym. Chem.*, 2016, **7**, 926–932.
- 35 Y. Lim, S.-G. Ihn, X. Bulliard, S. Yun, Y. Chung, Y. Kim, H. Chang and Y. S. Choi, *Polymer*, 2012, **53**, 5275–5284.
- 36 L. Ye, X. Jiao, S. Zhang, H. Yao, Y. Qin, H. Ade and J. Hou, *Adv. Energy Mater.*, 2016, **6**, 1601138.
- 37 H. Li, F. Liu, X. Wang, C. Gu, P. Wang and H. Fu, *Macromolecules*, 2013, **46**, 9211–9219.
- 38 Y. T. Chen, T. W. Huang, C. L. Wang and C. S. Hsu, *Polym. Chem.*, 2015, **6**, 3728–3736.
- 39 H. Xu, J. Li, J. Mai, T. Xiao, X. Lu and N. Zhao, *J. Phys. Chem. C*, 2014, **118**, 5600–5605.
- 40 K. H. Hendriks, G. H. L. Heintges, M. M. Wienk and R. A. J. Janssen, *J. Mater. Chem. A*, 2014, **2**, 17899–17905.
- 41 J. W. Jung, F. Liu, T. P. Russell and W. H. Jo, *Energy Environ. Sci.*, 2013, **6**, 3301–3307.
- 42 J. W. Lee, H. Ahn and W. H. Jo, *Macromolecules*, 2015, **48**, 7836–7842.
- 43 K. H. Kim, S. Park, H. Yu, H. Kang, I. Song, J. H. Oh and B. J. Kim, *Chem. Mater.*, 2014, **26**, 6963–6970.
- 44 J. W. Jung, J. W. Jo, E. H. Jung and W. H. Jo, *Org. Electron.*, 2016, **31**, 149–170.
- 45 W. Li, K. H. Hendriks, M. M. Wienk and R. A. J. Janssen, *Acc. Chem. Res.*, 2016, **49**, 78–85.
- 46 S. Qu and H. Tian, *Chem. Commun.*, 2012, **48**, 3039–3051.
- 47 L. Chen, D. Deng, Y. Nan, M. Shi, P. K. L. Chan and H. Chen, *J. Phys. Chem. C*, 2011, **115**, 11282–11292.
- 48 J. Yue, J. Liang, S. Sun, W. Zhong, L. Lan, L. Ying, W. Yang and Y. Cao, *Dyes Pigm.*, 2015, **123**, 64–71.
- 49 V. Govindan and C. G. Wu, *RSC Adv.*, 2017, **7**, 28788–28796.
- 50 J. Kuwabara, N. Takase, T. Yasuda and T. Kanbara, *J. Polym. Sci., Part A: Polym. Chem.*, 2016, **54**, 2337–2345.
- 51 C. B. Nielsen, M. Turbiez and I. McCulloch, *Adv. Mater.*, 2013, **25**, 1859–1880.
- 52 Z. Yi, S. Wang and Y. Liu, *Adv. Mater.*, 2015, **27**, 3589–3606.
- 53 C. Kanimozhi, P. Balraju, G. D. Sharma and S. S. Patil, *J. Phys. Chem. B*, 2010, **114**, 3095–3103.
- 54 P. Shen, H. Bin, L. Xiao and Y. Li, *Macromolecules*, 2013, **46**, 9575–9586.
- 55 M. Brumbach, D. Placencia and N. R. Armstrong, *J. Phys. Chem. C*, 2008, **112**, 3142–3151.
- 56 Y. Zhu, R. D. Champion and S. A. Jenekhe, *Macromolecules*, 2006, **39**, 8712–8719.
- 57 C. B. Nielsen, M. Turbiez and I. McCulloch, *Adv. Mater.*, 2013, **25**, 1859–1880.
- 58 M. J. Frisch, G. W. Trucks, H. B. Schlegel, G. E. Scuseria, M. A. Robb, J. R. Cheeseman, G. Scalmani, V. Barone, B. Mennucci and G. A. Petersson, *et al.*, *GAUSSIAN 09, Revision A.02*, Gaussian, Inc., Wallingford, CT, 2009.
- 59 M. E. Reish, S. Nam, W. Lee, H. Y. Woo and K. C. A. Gordon, *J. Phys. Chem. C*, 2012, **116**, 21255–21266.
- 60 Y. Li, P. Sonar, S. P. Singh, M. S. Soh, M. V. Meurs and J. Tan, *J. Am. Chem. Soc.*, 2011, **133**, 2198–2204.
- 61 J. S. Ha, K. H. Kim and D. H. Choi, *J. Am. Chem. Soc.*, 2011, **133**, 10364–10367.
- 62 M. Shahid, R. S. Ashraf, Z. Huang, A. J. Kronemeijer, T. C. Ward, I. McCulloch, J. R. Durrant, H. Sirringhaus and M. Heeney, *J. Mater. Chem.*, 2012, **22**, 12817–12823.
- 63 M. C. Scharber, D. Mühlbacher, M. Koppe, P. Denk, C. Waldauf, A. J. Heeger and C. J. Brabec, *Adv. Mater.*, 2006, **18**, 789–794.
- 64 T. E. Kang, J. Choi, H. H. Cho, S. C. Yoon and B. J. Kim, *Macromolecules*, 2016, **49**, 2096–2105.
- 65 H. Choi, S. J. Ko, T. Kim, P. O. Morin, B. Walker, B. H. Lee, M. Leclerc, J. Y. Kim and A. J. Heeger, *Adv. Mater.*, 2015, **27**, 3318–3324.
- 66 S. K. Son, Y. S. Kim, H. J. Son, M. J. Ko, H. Kim, D. K. Lee, J. Y. Kim, G. H. Choi, K. Kim and B. Kim, *J. Phys. Chem. C*, 2014, **118**, 2237–2244.
- 67 A. Gopal, A. Saeki, M. Ide and S. Seki, *ACS Sustainable Chem. Eng.*, 2014, **2**, 2613–2622.
- 68 C. V. Hoven, X. D. Dang, R. C. Coffin, J. Peet, T.-Q. Nguyen and G. C. Bazan, *Adv. Mater.*, 2010, **22**, E63–E66.